



# LUND UNIVERSITY

## Spatiotemporal and microstructural characterization of heterotopic ossification in healing rat Achilles tendons

Pierantoni, Maria; Hammerman, Malin; Silva Barreto, Isabella; Larsson, Daniel; Notermans, Thomas; Bodey, Andrew J.; Eliasson, Pernilla; Isaksson, Hanna

*Published in:*  
FASEB Journal

*DOI:*  
[10.1096/fj.202201018RRR](https://doi.org/10.1096/fj.202201018RRR)

2023

*Document Version:*  
Peer reviewed version (aka post-print)

[Link to publication](#)

*Citation for published version (APA):*  
Pierantoni, M., Hammerman, M., Silva Barreto, I., Larsson, D., Notermans, T., Bodey, A. J., Eliasson, P., & Isaksson, H. (2023). Spatiotemporal and microstructural characterization of heterotopic ossification in healing rat Achilles tendons. *FASEB Journal*, 37(6), Article e22979. <https://doi.org/10.1096/fj.202201018RRR>

*Total number of authors:*  
8

### General rights

Unless other specific re-use rights are stated the following general rights apply:  
Copyright and moral rights for the publications made accessible in the public portal are retained by the authors and/or other copyright owners and it is a condition of accessing publications that users recognise and abide by the legal requirements associated with these rights.

- Users may download and print one copy of any publication from the public portal for the purpose of private study or research.
- You may not further distribute the material or use it for any profit-making activity or commercial gain
- You may freely distribute the URL identifying the publication in the public portal

Read more about Creative commons licenses: <https://creativecommons.org/licenses/>

### Take down policy

If you believe that this document breaches copyright please contact us providing details, and we will remove access to the work immediately and investigate your claim.

LUND UNIVERSITY

PO Box 117  
221 00 Lund  
+46 46-222 00 00



**Spatiotemporal and microstructural characterization of heterotopic ossification in healing rat Achilles tendons**

Maria Pierantoni<sup>1</sup>, Malin Hamnerman<sup>2</sup>, Isabella Silva Barreto<sup>1</sup>, Daniel Larsson<sup>1</sup>, Thomas Notermans<sup>1</sup>, Andrew J. Bodey<sup>3</sup>, Pernilla Eliasson<sup>2\*</sup>, Hanna Isaksson<sup>1\*</sup>

<sup>1</sup>. Department of Biomedical Engineering, Lund University, Box 118, 221 00 Lund, Sweden

<sup>2</sup>. Department of Biomedical and Clinical Sciences, Linköping University, 581 83 Linköping, Sweden

<sup>3</sup>. Diamond Light Source, Didcot, Oxfordshire, OX11 0DE, UK

\*equal last authorship

**To whom correspondence should be addressed:**

Maria Pierantoni, PhD

Department of Biomedical Engineering

Lund University / LTH

Box 118, 221 00 Lund, Sweden

E-mail: [maria.pierantoni@bme.lth.se](mailto:maria.pierantoni@bme.lth.se)

The authors declare that there are no conflicts of interest in connection with this article.

30

## **Abstract**

Achilles tendon rupture is a common debilitating medical condition. The healing process is  
33 slow and can be affected by heterotopic ossification (HO), which occurs when pathologic bone-  
like tissue is deposited instead of the soft collagenous tendon tissue. Little is known about the  
temporal and spatial progression of HO during Achilles tendon healing. In this study we  
36 characterize HO deposition, microstructure, and location at different stages of healing in a rat  
model. We use phase-contrast enhanced synchrotron micro-tomography, a state-of-the-art  
technique that allows 3D imaging at high-resolution of soft biological tissues without invasive  
39 or time-consuming sample preparation. The results increase our understanding of HO  
deposition, from the early inflammatory phase of tendon healing, by showing that the  
deposition is initiated as early as one week after injury in the distal stump and mostly growing  
42 on pre-injury HO deposits. Later, more deposits form first in the stumps and then all over the  
tendon callus, merging into large, calcified structures which occupy up to 10% of the tendon  
volume. The HOs were characterized by a looser connective trabecular-like structure and a  
45 proteoglycan rich matrix containing chondrocyte-like cells with lacunae. The study shows the  
potential of 3D imaging at high-resolution by phase contrast tomography to better understand  
-ossification in healing tendons.

48

**Keywords:** pathologic calcification, synchrotron imaging, endochondral, mineralization  
template

51

## Introduction

Tendon and ligament injuries represent one of the most common musculoskeletal pathologies for which patients require medical care [1,2]. Achilles tendon repair after injury or rupture is a very slow process. The poor intrinsic healing capacity is considered to be, in part, due to the low cellularity and vascularity in the tendon tissue, but our understanding of the repair process is still limited [2,3]. During repair, different types of tendon cells proliferate and synthesize collagen and other extracellular matrix proteins to reform collagen fibrils and fibers. Injured tendons do not seem to fully regain their original structural and biomechanical properties such as strength, flexibility, and elasticity [4–6].

One complication associated with tendon healing and tendinopathy is heterotopic ossification (HO). HO is an aberrant regenerative process in which pathologic bone is deposited where it should normally not be present, in this case in the soft tendon tissue [7]. HO may be triggered in response to musculoskeletal trauma by differentiation of stem cells or tendon cells into chondrocytes which can form cartilage, undergo hypertrophy and calcify into bone-like deposits [7,8]. Recent studies indicate that HO deposition may share similar mechanisms with normal physiological osteogenesis [9]. However, other studies suggest that although HO formation can involve osteoblasts and osteoclasts, the deposition greatly differs from physiological osteogenesis and can vary depending on the origin of the HO [10].

HO can result in pain and dysfunction, and thus may severely affect the life quality of patients [11]. A recent clinical study has shown that almost 20% of the patients with a surgically repaired Achilles tendon rupture have some level of HO in their healing Achilles tendon [12]. The formation of the HO after tendon rupture appears to be an early process initiated within the first six weeks and can then be visualized by plain x-ray.

Small animal models play a fundamental role in tendon research, especially for mechanistic investigation where human studies are impossible [13]. In particular, rats provide a model

78 where tendon studies are fast and reproducible, while still being important for human tendon  
physiology and healing [1,14]. HO during tendon healing in rats is even more common than in  
humans and areas of cartilage and ossified tissue were recently observed after 3 to 17 and 5 to  
81 16 weeks of healing [3,7,15–19]. However, there is limited knowledge about HO in relation to  
Achilles tendon healing and the specific spatiotemporal evolution of HO during tendon  
regeneration. In order to study how the collagenous tendon tissue is mineralized, it is important  
84 to use techniques that allow 3D visualization at high resolution and quantification [20]. Here  
we use a rat model in combination with high-resolution phase contrast enhanced synchrotron  
X-ray tomography to improve our understanding of the spatiotemporal formation of HO in  
87 healing Achilles tendons. This study provides new insights on the formation, microstructure,  
and growth mechanism of HO deposits.

## 90 2. Methods

### 2.1 Animal model

The right Achilles tendon of 29 female Sprague-Dawley rats (12 weeks old) was transected  
93 transversely under sedation with isoflurane, as previously described [19,21]. During the healing  
period, the rats were kept two per cage, free to move around, with a light-dark cycle of 12 hours  
and controlled temperature (22 °C). Food and water were provided *ad libitum*. The rats were  
96 euthanized at 1, 2, 3, 6, 12, 16 and 20 weeks post-injury. The tendons were dissected and  
harvested for either tomography (all time points) or for histology (12 and 20 weeks). The study  
was approved by the Regional Ethics Committee for animal experiments in Linköping, Sweden  
99 (Jordbruksverket, ID1424).

## 2.2 Synchrotron phase contrast X-ray tomography

Samples from all time points (week 1: N=4, week 2: N=1, week 3: N=4, week 6: N=2, week 12: N=4, week 16: N= 2, week 20: N=4) were stored frozen in saline solution (-20°C) until imaging. Additionally, a contralateral intact tendon of one 3 weeks healing rat was imaged as controls for the short healing time points and two contralateral tendons of the 20 weeks as controls for the long healing samples. All samples were imaged by synchrotron phase contrast X-ray tomography at the Diamond-Manchester Imaging Branchline I13–2 [22,23] of the Diamond Light Source (DLS) synchrotron (Oxfordshire, United Kingdom). A partially-coherent, near-parallel, polychromatic ‘pink’ beam (8 – 30 keV) was generated by an undulator in an electron storage ring of 3.0 GeV voltage and 300 mA current. Samples were kept frozen throughout the scans using an Oxford Cryosystems nitrogen jet (Fig. 1A). Temperature was set to 84 K and the cooling jet was directed towards the sample from above. Keeping the sample frozen during the scans limited sample movement and prevented bubbling of the saline solution in which the samples were kept hydrated. Various propagation distances were tested, and ~400 mm was chosen to give the best level of phase contrast for the unstained soft tissues. 2001 projection images were acquired at equally-spaced angles over 180° of continuous rotation (‘fly scan’). Dark- and flat-field images were collected to normalize projections. Images were collected by a pco.edge 5.5 Camera Link (PCO AG, Germany) detector (sCMOS sensor of 2560 × 2160 pixels) mounted on a visible light microscope of variable magnification. A 1.25× objective coupled to a 500µm LuAG:Ce scintillator that was mounted ahead of a 2× lens, provided 2.5× total magnification with a field of view of 6.7 × 5.6 mm and an effective pixel size of 2.6 µm. Exposure time was 50ms (overhead 11ms), leading to imaging times of circa 2.5 minutes per tomographic data collection (~130s total exposure). To cover the whole tendon from heel bone to muscles, 2 to 3 consecutive vertical scans were acquired, while keeping an overlap between consecutive scans of 10%. 3D volumes were reconstructed via filtered back

projection in the modular pipeline Savu [24,25] which incorporated flat- and dark-field  
 129 correction, optical distortion correction [26,27], ring artefact suppression [28] and automatic  
 rotation center calculation [29].

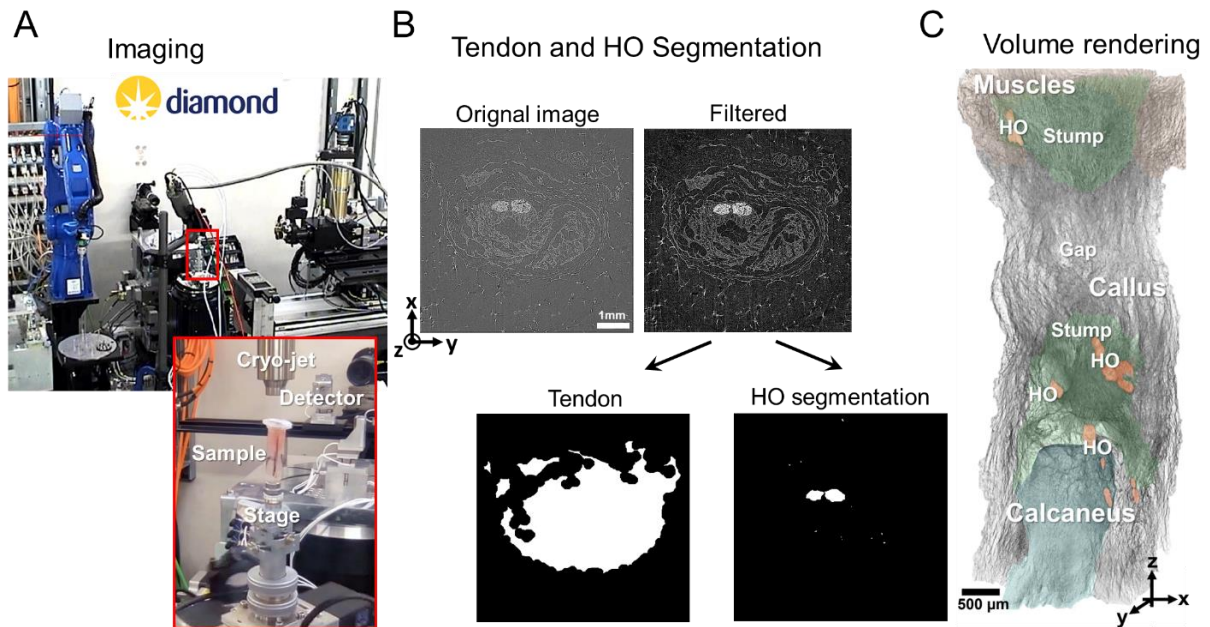


**Figure 1. Experimental workflow for Synchrotron Phase contrast X-Ray Tomography.** A) Imaging setup at I13-2, Diamond Light Source. A cryojet enabled to image the samples while keeping them frozen; B) automatic image processing to segment tendon soft tissue and HO deposits; C) volume rendering showing different components in a healing tendon (week 6).

## 2.3 Image analysis

Segmentation and quantification: A MATLAB custom made pipeline for volume segmentation was designed to select tendon soft tissue and HO deposits (Fig. 1B). The full resolution image stacks were preprocessed by filtering with CLAHE- and Median-filters and subtracting the image background. Then the tendon tissue was binarized using the Otsu's method. The selection was denoised by applying a size filter that removed all features smaller than  $2.5 \times 10^{-4} \text{ mm}^3$ . To enable segmentation of the soft tendon, gaps were filled in 3D. To achieve this, morphological operations of closing and opening were performed in sequence first in the XY plane then in the XZ plane (structural element: disk of 2 to 50 pixels depending on the iteration step). HO deposits were selected by threshold segmentation increasing the value used for the



soft tissue of ~10 times. The tendon total volume was calculated as the sum of white pixels. The total volume of HO deposits was obtained as the sum of individual HO volumes and the percentage of tendon tissue occupied by HO deposits (HO volume fraction) was calculated as total volume of HO deposits divided by the total tendon volume (HO/tendon volume-ratio). The tendon length was calculated as the distance between the heel bone (tendon-bone junction) and the muscles (tendon-muscle junction). The gap length represents the distance between the upper and lower intact stumps (Fig. 1C).

Volume renderings of whole tendons were performed in ImageJ and Dragonfly (v 4.1, ORS software) [30,31]. To visualize the whole tendons (Fig. 1C), volumes were converted from 32-bit to 8-bit images and downsized 5 times, then all volumes were stitched using the BigStitcher plugin for ImageJ [32]. Dragonfly was used to manually segment part of the volumes to validate the automatic segmentation.

### 2.3.3 Validations

Comparison between tendons imaged at room temperature and while kept frozen: For this comparison, 2 samples were scanned both at room temperature (as described in details in [33]) and frozen according to the protocol described in the current study. Volume segmentation was performed manually using the Dragonfly software. The tendon tissues were selected manually every 100 slices (transversal tendon cross-section) and interpolated in between, along the tendon main axes. This volume segmentation was performed twice for each tendon sample: one when the tendon was imaged at room temperature and one when it was frozen (Fig. S1). The analysis showed that after freezing no changes in the total sample volume were observed (~1% difference between the volumes for the same sample frozen and at room temperature). However, the volumes of the individual fibers were reduced substantially by freezing, probably due to the formation of ice crystals in between them (Fig. S1 arrows).

Comparison between automatic and manual segmentation: The efficiency of the automatic segmentation was tested comparing the results obtained for subvolumes extracted from one intact and one healing tendon (Fig. S2). The whole tendon cross-section for 0.5 mm along the tendon main axes was considered. The difference between the two techniques was between 2% for the intact tendon and 5% for the healing tendon.

## 2.4 Histology

Healing Achilles tendons for histology were harvested after 3 (N=4), 12 (N=4) and 20 (N=4) weeks, treated with sucrose solution, snap-frozen in optimal cutting temperature compound (OCT; VWR international AB, Spånga, Sweden) in liquid nitrogen, as described previously [34]. The tendons were stored at -80°C before they were sectioned longitudinally comprising the full length of the tendon (7 µm thickness). Tendons were stained with hematoxylin & eosin to visualize tissue and cell morphology, and nuclear fast red & alcian blue to visualize proteoglycan content. The stained specimens were examined using an Olympus BX51 light microscope.

## 3. Results

### 3.1. 3D structural characterization of HO deposits during healing

Phase-contrast enhanced synchrotron micro-tomography allowed to clearly distinguish tendon and muscle structures, calcaneus bone and HO deposits (Fig. 1B) and to study the spatiotemporal evolution of HO during healing (Fig. 2). Small deposits of HO were initially found only in the distal stump close to the calcaneal bone (at 1-3 weeks) and not within the callus tissue. Thereafter (at 6-12 weeks), HO was also found in the proximal stump close to the muscles. At even later healing time points (16-20 weeks), HO was deposited nearly everywhere in the tendon (both at the stumps and in callus).

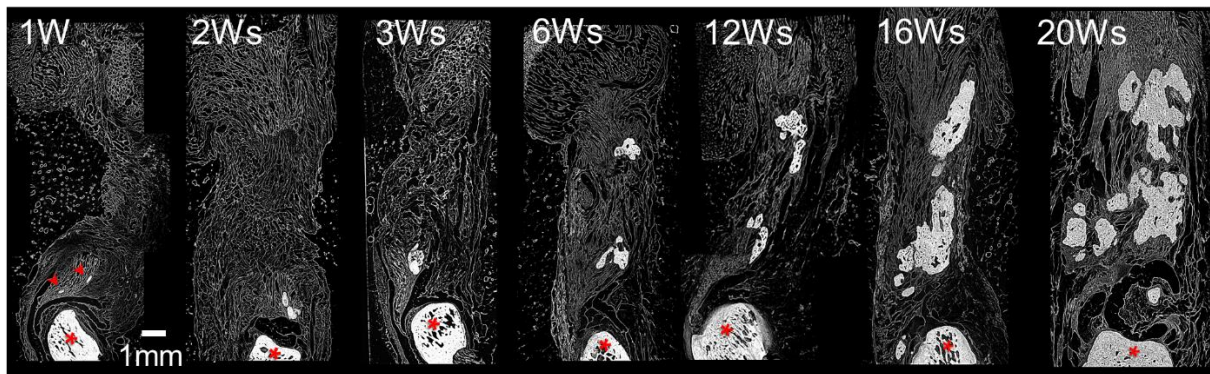


**Figure 2. Spatiotemporal evolution of HO deposits during tendon healing**, where the calcaneal bone is on the lower end (stars) and the muscle on the top, and the regenerating tendon in between. At 1-3 weeks of healing the HO deposits are shown as small white structures located close to the calcaneal bone (arrowheads), during healing they grow into bigger structures and at 20 weeks, HOs are widespread throughout the whole tendon.

We also observed small HO areas in all contralateral tendons (imaged as intact controls) close to the calcaneal bone, typically on the anterior side of the tendon (Fig. 3A left). This location is similar to the initial findings of HO in the healing tendons at 1 week. The HO deposits in the intact tendons were all characterized by a compact fiber-like structure (Fig. 3A right). At early healing time points (1-3 weeks) the additional HO deposition seemed to occur in relation to the pre-injury HO growing around it (Fig. 3B and Fig.S3). The HOs deposited during healing were characterized by a looser connective trabecular-like structure (Fig. 3B star). At 6 weeks, HO started spreading in new regions of the healing tendon where no pre-injury HOs were present: first close to the distal stump and then at the proximal stump (Fig. 2). By week 12, HO was forming also in the callus tissue (between the stumps, Fig. 2). At this point, the HO deposits were highly irregular, and often included fat-like tissue (Fig. 3C). Furthermore, starting from week 12, abundant regenerated tissue had formed in the gap making it difficult to distinguish the stumps from the rest of the callus tissue. At week 16, multiple HO deposits started to merge into one complex ossified structure and expanded toward the center of the tendon (Fig. 2 and Fig. 3D). By week 20, many HO deposits had merged into one denser structure with small fat inclusions (Fig. 2).

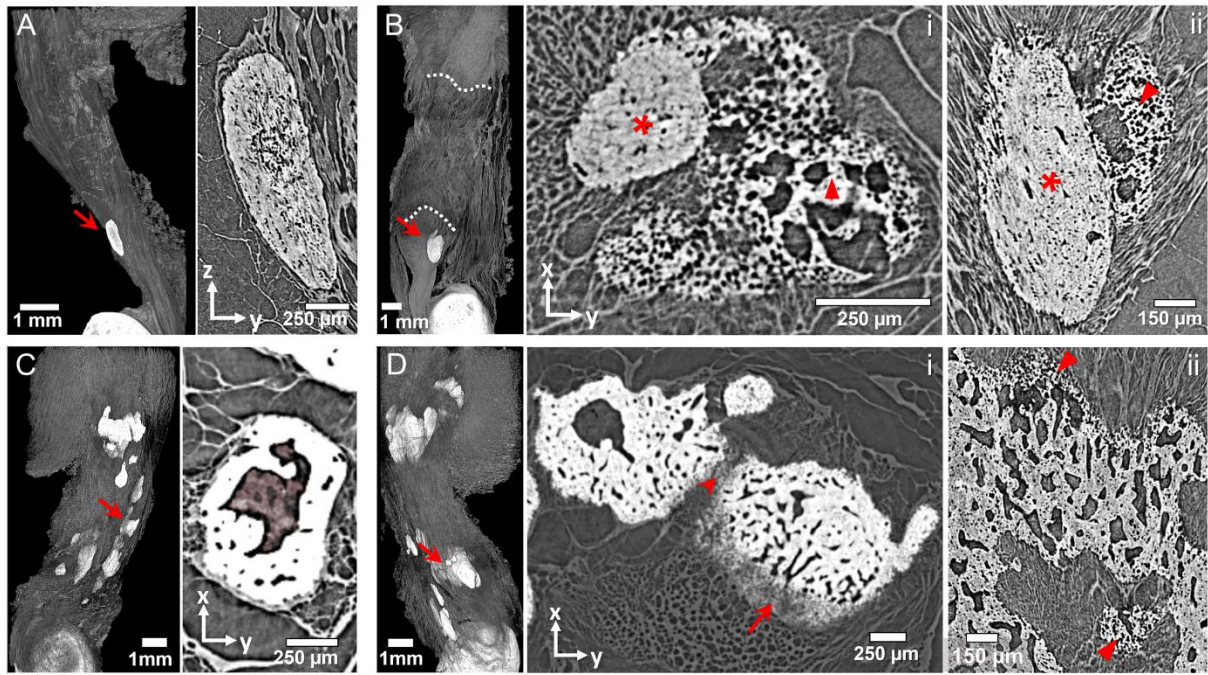


**Figure 3. Characterization of HO deposits.** In each subfigure on the left a volume rendering of the whole tendon shows the location of the HO deposit rendered at higher magnification on the right. A) HO in an intact tendon; B) HO in a 3-week healing tendon (the dotted lines indicate the stumps, \* indicate a pre-existing HO and the triangle the trabecular-like structure, i) cross sectional and ii) longitudinal views; C) Fat deposits (highlighted in red) enclosed in a HO deposit at 12 weeks; D) Multiple HO deposits start to merge (arrowhead) and grow outward (arrow) at 16 weeks of healing i) cross sectional and ii) longitudinal views, the triangles indicate the growth front.

### 3.2. Quantification of HO properties during healing

The volume of the tendon increased during the initial 3 weeks of healing to later decrease (Fig. 4A). In contrast the volume of the HO deposits grew substantially starting from 3 weeks onwards (Fig. 4A and B). The length of the tendon and the length of the gap between the intact stumps did not substantially change (Fig. 4C).

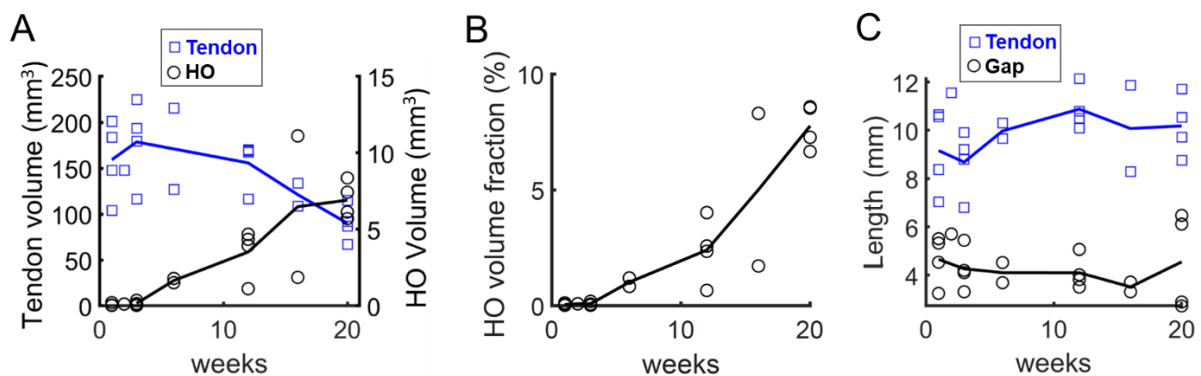


**Figure 4. Quantification of tendon and HO properties and their evolution during healing.** A)

Tendon tissue and HO volumes, B) HO volume fraction calculated as HO volume/ tendon volume and C) tendon and gap length.

### 3.3. Histological characterization of HO deposits and tendon tissue

Very early stages of HO, possibly preceding mineral deposition, were identified in 3-weeks healing tendons at the edge of the upper stump (Fig. 5A-D). This region was characterized by increased cellularity (Fig. 5A) including chondrocyte-like cells being more rounded and bigger than the surrounding tendon cells (Fig. 5B). As seen with alcian blue staining, this region was also characterized by a slightly higher proteoglycan content than the surrounding tissue (Fig. 5C, D). This area coincides with regions where large deposits were found at later time points during healing (Fig. 5E).

Furthermore, after being imaged by tomography, a 3-week healing tendon containing a pre-existing deposit was embedded and stained with hematoxylin and eosin. The pre-existing deposit was identified and imaged showing a fiber-like structure equivalent to the structure that could be observed by tomography (Fig. S4). At 12 and 20 weeks the HO appeared as dark purple in hematoxylin & eosin staining (Fig. 5E, F, I, J), and dark blue (especially at the borders) in alcian blue staining (Fig. 5G, H, K, L). These HO regions contained either high (12 weeks, Fig. 5G, H) or low-level of proteoglycans (20 weeks, Fig 5 K, L), but all contained acellular areas, lined with cells (Fig. 5G, H, K, L). Chondrocyte-like cells with lacunae could often be identified in proteoglycan-rich regions (Fig. 5G, H). The stumps were easily distinguishable from healing tissue both at 12 and 20 weeks of healing (Fig. 5I).



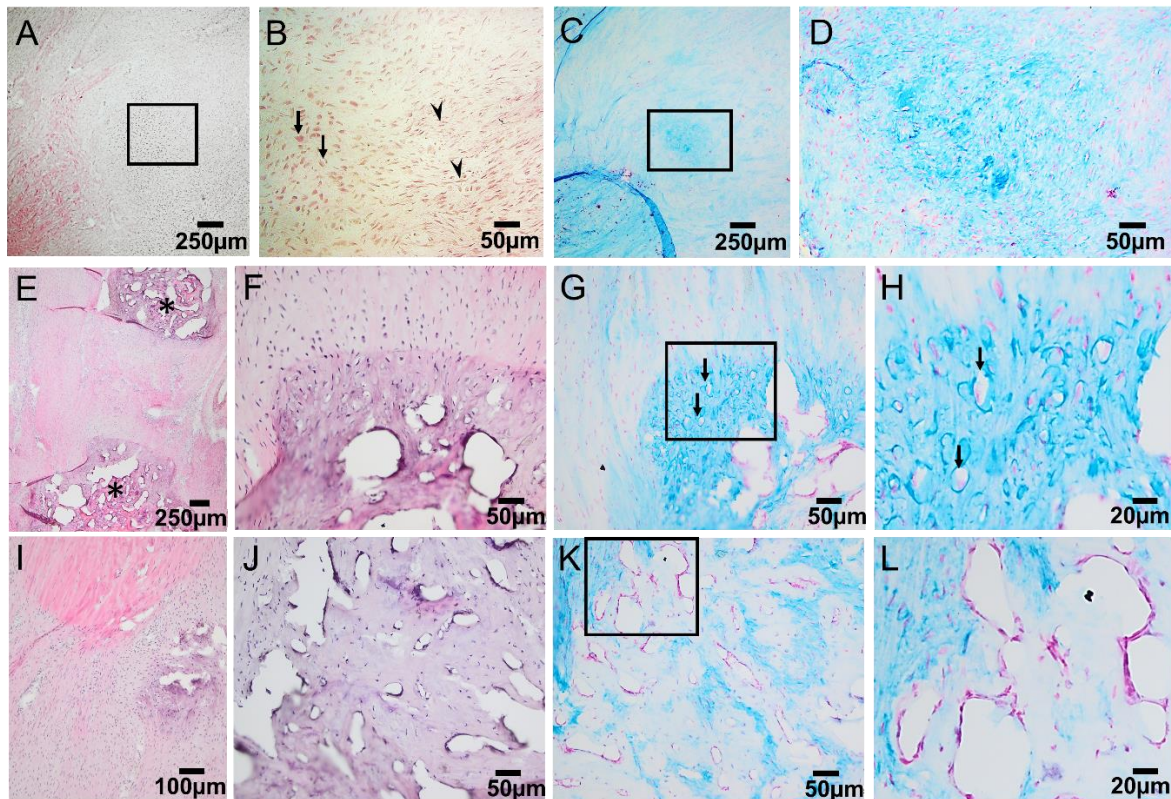


**Figure 5. Histology of HO regions in healing tendons at 3, 12 and 20 weeks.** Healing tendons were stained with hematoxylin & eosin (A-B, E-F, I-J) or nuclear fast red & alcian blue (C-D, G-H, K-L). A) Region showing early stages of HO at the stump in a 3-weeks healing tendon. B) Magnification of the transition between a HO area characterized by round wide cells (arrows) and the surrounding tendon-like tissue (characterized by elongated and smaller cells, arrowheads), as marked in A.). C) The same sample and similar region as in A showing that the proteoglycan content is slightly higher (rectangle) in the HO region than in the surrounding tissue. D) Magnification of the area marked in C. E) Healing tendon at 12 weeks including two HO regions (dark purple, \*), one at each stump. F) HO region with high proteoglycan content and chondrocyte-like cells in a 12-weeks healing tendon. G) The same sample and similar region as in F. Cell lacunae (arrows) indicate the presence of chondrocytes. H) Magnification of the marked area in G showing the interface between the HO region and the soft tendon tissue. I) Healing tendon at 20 weeks showing a stump (dark pink) with one HO region (dark purple). J) HO region with low proteoglycan content. K) The same sample and similar region as in J. L) Magnification of the area marked in K showing the border between the HO region and the soft tendon tissue.

## Discussion

By using high-resolution phase-contrast synchrotron X-ray tomography this study provides new information on the spatiotemporal formation, structure, and growth of HO deposits in healing rat Achilles tendons. We identified HO deposits with fiber-like internal structure (visible both in the tomograms, Fig. 3) close to the calcaneal bone in all the intact tendons similarly to what we recently reported [35]. The fiber-like structure allowed us to distinguish

the pre-existing deposits from HO formed during the healing process [35]. The pre-existing  
282 HO deposits were also clearly visible at 1 week, and the size (in some cases up to  $1.2\text{mm}^3$ ) was  
comparable to what we observed in intact tendons [35] however, new mineral deposition at  
some of the edges could be already observed (Fig. S3). Moreover, we did not observe an  
285 increase in size or number of this fiber-like HO deposit structure during the healing process,  
but they seemed to act as templates for additional mineral formation. In fact, at early healing  
time points, HO was observed only where these pre-existing fiber-like deposits are located.  
288 The HO deposited during healing had a more trabecular-like structure, and the histological  
results show chondrocytes and proteoglycan rich matrix. It was previously shown for hip, knee,  
brain and spinal cord that, when HO is associated with trauma, the deposition occurs primarily  
291 through endochondral osteogenesis [36]. Our results also suggest that in rat Achilles tendons,  
HO post-injury occurs through endochondral ossification. Previous studies have shown that  
BMP signaling in general, and the activin receptor type-1 (Acvr1) in particular, seem to be  
294 involved in endochondral ossification and HO [10,37]. Furthermore, both inflammation and  
mechanical loading have been suggested to contribute to HO, possibly through stimulation of  
mTORC1 and activation of quiescent stem cells [38–40]. Blocking of this pathway by  
297 rapamycin has been shown to prevent traumatic HO deposition in a mouse model for Achilles  
tendon injury, and could represent a possible therapeutic factor against HO [10]. Additionally,  
HO could result from stem cell or progenitor cell differentiation, specifically from a group of  
300 cathepsin K positive tendon progenitor cells [41]. However, additional in-depth studies on  
cellular contributions to HO and interventions to prevent HO after tendon rupture is needed,  
and we suggest that phase-contrast enhanced synchrotron micro-tomography could be used to  
303 evaluate the tissue in such studies.

Earlier animal studies have demonstrated HO deposition after 3 to 5 weeks of tendon healing  
[7,17]. However, we have shown initiation of the ossification already at 1 week post-injury

(Fig. S3), and possibly even earlier. This observation extends our knowledge regarding HO deposition during the inflammatory phase of tendon healing. However, at the early stages of healing the HO deposits were not found in the immediate callus tissue, but rather in the stumps. Our results show that from 6 weeks and onwards, HO deposits also formed in regions where there were no pre-injury deposits, first in the distal stump and then in the proximal stump. This is consistent with human data where HO is primarily formed outside the callus area [12]. Furthermore, in the upper stump, where deposits were observed at 6 weeks, histology showed regions with slightly higher proteoglycan content than surrounding tissue and the presence of chondrocyte-like cells at this site already at 3 weeks (Fig. 5A-D). This possibly represents an early stage of HO preceding mineral deposition. However, to confirm this observation, more samples and time points should be considered.

The observed increase in proteoglycans may represent an initiation of HO formation; thus, a phase that is preceding the mineral deposition. These results were also in good agreement with previous observations in animal studies of cartilage, proteoglycans and other indicators of HO or endochondral ossification being present near the stumps from around 4 weeks of healing [17,19,50]. Previous literature has also suggested that tissue vascularization precedes HO [51,52]. Consequently, one of the reasons why HO formation was first observed in the stumps and only later in the gap tissue could be the initial lack of oxygenation in the callus tissue. Furthermore, our data indicated that the total tendon volume increased until 3 weeks and then started to decrease. This can be explained as the two initial phases of tendon healing are associated with inflammation and bulk matrix production and the third phase, the remodeling is associated with a volume reduction [21]. Additionally, the gap between the intact stumps did not seem to change over time.

By week 12, HO deposition occurred also in the center of the callus area, between the stumps, with a more irregular structure where often fat inclusions were found within the HO. Abundant



fat deposition embedded in the callus was also observed during the early stages of healing. Fat tissue in healing tendons has previously been described in other studies, but not encapsulated in HO deposits [19,53]. The spheric deposits that we observed are similar to the fat tissue also observed around intact tendons [33] and within some of the HO protruding out from intact tendons [35]. The presence of fat-like tissue inside some HO could explain previous histological observation of unstained regions (and consequently neither mineral nor cartilage) in the center of some deposits at weeks 12 and 16 [8], and the presence of the empty rings observed in histological images in this study at weeks 12 and 20. In previous studies, vessels were detected in the large ossified areas after 12 and 16 weeks of healing [8,54]. HO may be associated with vascularization, higher oxygen supply and increased mechanical stimulation [39,54], while a reduction in oxygen levels and low mechanical stimulation may lead to reduced amounts of HO and increased presence of adipose tissue [53]. Adipose tissue in the healing region may be less debilitating than HO, and result in more successful healing outcomes compared to when HO is formed [55]. Furthermore, histology shows a lower presence of chondrocytes at week 20 than at week 12, which could indicate that most regions with cartilaginous tissue have ossified by 20 weeks and that the rate of the HO deposition started to decrease. However, this cannot be confirmed as we did not consider timepoints beyond 20 weeks. This study only used female rats as they grow slower than male rats. Therefore, as a limitation we cannot study sex specific differences. Furthermore, as an additional limitation of this study, histology was mainly performed at late time points (12 and 20 weeks) when many bigger deposits, that were easy to identify, were present. In the future, histological studies of the initial stages of HO formation at early healing time points would be highly beneficial to better understand the underlying biology of the initiation process of HO. HO deposits in healing Achilles tendons are not unique to rats. They are also common in humans most often on the anterior side of the healing tendon [12]. Approximately 20% of

patients with Achilles tendon rupture can develop HO [12,56]. The impact of the HO on patient functional outcomes are inconclusive, but large HO deposits have been hypothesized to contribute to poor function after tendon repair [12,17]. When reviewing clinical CT images from 38 patients enrolled in a clinical trial [12], we found some similarities between HO deposits in rats and humans. In both rats and humans, the HO deposits at early healing have an elongated morphology which extends in the direction of the tendon main axes. Furthermore, HOs are more commonly located in the correspondence of the lower stump close to the calcaneus, and they are often at the border of the tendon stump, almost bulging out from it (Fig. 3B and Fig. 6).

Starting from the 1990s several studies have investigated the advantages of using synchrotron X-ray for radiography, radiotherapy and clinical diagnostics [42–44]. A significant dose reduction for equivalent image quality could be reached using synchrotron monochromatic radiation [43,45]. To date, there are still researchers that continue to push forward the use of synchrotron beamlines for clinically focused research [45,46]. However, the synchrotron X-ray tomography approach used in this study cannot be used as a diagnostic tool and can only be performed ex vivo and on a limited number of samples. Nevertheless, we believe that the presented results can pave the way for future studies using high-resolution synchrotron X-ray tomography to understand HO progression during tendon healing. In particular, high resolution structural characterization, in conjunction with a precise localization of HO, could in future allow to create a classification system for HO deposits in tendons and ligaments based on location, size, and morphology of the deposits similar to the Della Valle and Brooker classifications for HO formation following total hip arthroplasty [47–49].

## Conclusions

HO in healing Achilles tendons is a prevalent clinical problem. This study shows that by using 3D high-resolution phase-contrast synchrotron X-ray tomography new understanding of the pathological process by which HO deposits form can be gained. Our results indicate that both ossification on pre-existing HO and endochondral ossification may occur, but at different healing time points. Additionally, the spatial evolution of the deposits, occurring first in the lower stump, then close to muscles and only at later time points in the centre of the callus, as well as the presence of encapsulated fat, could give insights on the factors governing HO.

## **Acknowledgments**

Funding from the Knut and Alice Wallenberg KAW Foundation (Wallenberg Academy Fellows 2017.0221) the European Research Council (ERC) under the European Union's Horizon 2020 research and innovation programme (grant agreement No 101002516), the Swedish research council (2017-00990), the Royal Physiographic Society of Lund (41380) and the Greta and Johan Kocks fondation (188\_20201015\_071) are greatly acknowledged. We thank Diamond Light Source for providing beamtime at the Diamond-Manchester Imaging Branchline I13-2 (proposal MT16557) and Dr. David Eastwood and Dr. Shashidhara Marathe for assistance with data collection.

## **Data Availability Statement**

The dataset on which this paper is based is too large to be retained or publicly archived with available resources. However, the data that support the findings of this study are available on request from the corresponding author.

## **Author Contributions**

M. Pierantoni, P. Eliasson and H. Isaksson conceptualization, investigation, and founding; M.

Pierantoni writing of the original draft; M. Pierantoni, M. Hammerman, and I. Silva Barreto

data acquisition, M. Pierantoni and A. J. Bodey methodology; M. Pierantoni and Daniel

Larsson analysis; M. Hammerman, I. Silva Barreto and T. Notermans validation, data curation

and review & editing; A. J. Bodey, P. Eliasson and H. Isaksson resurces; P. Eliasson

and H. Isaksson supervision, review & editing.

## References

- [1] J.G. Snedeker, J. Foolen, Tendon injury and repair - A perspective on the basic mechanisms of tendon disease and future clinical therapy, *Acta Biomater.* 63 (2017) 18–36.  
<https://doi.org/10.1016/j.actbio.2017.08.032>.
- [2] P. Sharma, N. Maffulli, Tendon injury and tendinopathy: healing and repair, *J. Bone Joint Surg. Am.* 87 (2005) 187–202. <https://doi.org/10.2106/JBJS.D.01850>.
- [3] T. Sakabe, T. Sakai, Musculoskeletal diseases--tendon, *Br. Med. Bull.* 99 (2011) 211–225.  
<https://doi.org/10.1093/bmb/ldr025>.
- [4] S. Tozer, D. Duprez, Tendon and ligament: development, repair and disease, *Birth Defects Res. Part C Embryo Today Rev.* 75 (2005) 226–236. <https://doi.org/10.1002/bdrc.20049>.
- [5] R.H. Gelberman, P.R. Manske, J.S. Vande Berg, P.A. Lesker, W.H. Akeson, Flexor tendon repair in vitro: a comparative histologic study of the rabbit, chicken, dog, and monkey, *J. Orthop. Res. Off. Publ. Orthop. Res. Soc.* 2 (1984) 39–48. <https://doi.org/10.1002/jor.1100020107>.
- [6] S. Asai, S. Otsuru, M.E. Candela, L. Cantley, K. Uchibe, T.J. Hofmann, K. Zhang, K.L. Wapner, L.J. Soslowsky, E.M. Horwitz, M. Enomoto-Iwamoto, Tendon Progenitor Cells in Injured Tendons Have Strong Chondrogenic Potential: The CD105-Negative Subpopulation Induces Chondrogenic Degeneration, *STEM CELLS.* 32 (2014) 3266–3277.  
<https://doi.org/10.1002/stem.1847>.
- [7] L. Lin, Q. Shen, T. Xue, C. Yu, Heterotopic ossification induced by Achilles tenotomy via endochondral bone formation: Expression of bone and cartilage related genes, *Bone.* 46 (2010) 425–431. <https://doi.org/10.1016/j.bone.2009.08.057>.
- [8] P.P.Y. Lui, L.S. Chan, Y.C. Cheuk, Y.W. Lee, K.M. Chan, Expression of Bone Morphogenetic Protein-2 in the Chondrogenic and Ossifying Sites of Calcific Tendinopathy and Traumatic Tendon Injury Rat Models, *J. Orthop. Surg.* 4 (2009) 27. <https://doi.org/10.1186/1749-799X-4-27>.
- [9] J.-M. Kim, Y.-S. Yang, K.H. Park, X. Ge, R. Xu, N. Li, M. Song, H. Chun, S. Bok, J.F. Charles, O. Filhol-Cochet, B. Boldyreff, T. Dinter, P.B. Yu, N. Kon, W. Gu, T. Takarada, M.B. Greenblatt, J.-H. Shim, A RUNX2 stabilization pathway mediates physiologic and pathologic bone formation, *Nat. Commun.* 11 (2020) 2289. <https://doi.org/10.1038/s41467-020-16038-6>.
- [10] Y. Xu, M. Huang, W. He, C. He, K. Chen, J. Hou, M. Huang, Y. Jiao, R. Liu, N. Zou, L. Liu, C. Li, Heterotopic Ossification: Clinical Features, Basic Researches, and Mechanical Stimulations, *Front. Cell Dev. Biol.* 10 (2022). <https://www.frontiersin.org/article/10.3389/fcell.2022.770931> (accessed February 25, 2022).
- [11] E.J.O. O'Brien, C.B. Frank, N.G. Shrive, B. Hallgrímsson, D.A. Hart, Heterotopic mineralization (ossification or calcification) in tendinopathy or following surgical tendon trauma, *Int. J. Exp. Pathol.* 93 (2012) 319–331. <https://doi.org/10.1111/j.1365-2613.2012.00829.x>.

450 [12] S.P. Magnusson, A.-S. Agergaard, C. Couppé, R.B. Svensson, S. Warming, M.R. Krogsgaard, M.  
Kjaer, P. Eliasson, Heterotopic Ossification After an Achilles Tendon Rupture Cannot Be  
453 Prevented by Early Functional Rehabilitation: A Cohort Study, *Clin. Orthop. Relat. Res.* 478  
(2020) 1101–1108. <https://doi.org/10.1097/CORR.0000000000001085>.

[13] B.J. Rigby, N. Hirai, J.D. Spikes, H. Eyring, The Mechanical Properties of Rat Tail Tendon, *J. Gen.  
Physiol.* 43 (1959) 265–283. <https://doi.org/10.1085/jgp.43.2.265>.

456 [14] T.L. Willett, R.S. Labow, I.G. Aldous, N.C. Avery, J.M. Lee, Changes in Collagen With Aging  
Maintain Molecular Stability After Overload: Evidence From an In Vitro Tendon Model, *J.  
Biomech. Eng.* 132 (2010). <https://doi.org/10.1115/1.4000933>.

459 [15] A. Misir, T.B. Kizkapan, Y. Arikan, D. Akbulut, M. Onder, K.I. Yildiz, S.E. Ozkocer, Repair within  
the first 48 h in the treatment of acute Achilles tendon ruptures achieves the best  
462 biomechanical and histological outcomes, *Knee Surg. Sports Traumatol. Arthrosc.* (2019).  
<https://doi.org/10.1007/s00167-019-05536-w>.

[16] F.S. da Silva, B.J. Abreu, B.I. Eriksson, P.W. Ackermann, Complete mid-portion rupture of the  
465 rat achilles tendon leads to remote and time-mismatched changes in uninjured regions, *Knee  
Surg. Sports Traumatol. Arthrosc.* 29 (2021) 1990–1999. <https://doi.org/10.1007/s00167-020-06239-3>.

[17] K. Howell, C. Chien, R. Bell, D. Laudier, S.F. Tufa, D.R. Keene, N. Andarawis-Puri, A.H. Huang,  
468 Novel Model of Tendon Regeneration Reveals Distinct Cell Mechanisms Underlying  
Regenerative and Fibrotic Tendon Healing, *Sci. Rep.* 7 (2017) 45238.  
<https://doi.org/10.1038/srep45238>.

471 [18] K. Zhang, S. Asai, M.W. Hast, M. Liu, Y. Usami, M. Iwamoto, L.J. Soslowsky, M. Enomoto-  
Iwamoto, Tendon mineralization is progressive and associated with deterioration of tendon  
474 biomechanical properties, and requires BMP-Smad signaling in the mouse Achilles tendon  
injury model, *Matrix Biol.* 52–54 (2016) 315–324.  
<https://doi.org/10.1016/j.matbio.2016.01.015>.

[19] H. Khayyeri, M. Hammerman, M.J. Turunen, P. Blomgran, T. Notermans, M. Guizar-Sicairos, P.  
477 Eliasson, P. Aspenberg, H. Isaksson, Diminishing effects of mechanical loading over time during  
rat Achilles tendon healing, *PLOS ONE*. 15 (2020) e0236681.  
<https://doi.org/10.1371/journal.pone.0236681>.

480 [20] Z. Zou, T. Tang, E. Macías-Sánchez, S. Sviben, W.J. Landis, L. Bertinetti, P. Fratzl, Three-  
dimensional structural interrelations between cells, extracellular matrix, and mineral in  
normally mineralizing avian leg tendon, *Proc. Natl. Acad. Sci.* 117 (2020) 14102–14109.  
483 <https://doi.org/10.1073/pnas.1917932117>.

[21] M. Hammerman, F. Dietrich-Zagonel, P. Blomgran, P. Eliasson, P. Aspenberg, Different  
mechanisms activated by mild versus strong loading in rat Achilles tendon healing, *PLOS ONE*.  
486 13 (2018) e0201211. <https://doi.org/10.1371/journal.pone.0201211>.

[22] C. Rau, U. Wagner, Z. Pešić, A.D. Fanis, Coherent imaging at the Diamond beamline I13, *Phys.  
Status Solidi A*. 208 (2011) 2522–2525. <https://doi.org/10.1002/pssa.201184272>.

489 [23] Z.D. Pešić, A.D. Fanis, U. Wagner, C. Rau, Experimental stations at I13 beamline at Diamond  
Light Source, *J. Phys. Conf. Ser.* 425 (2013) 182003. <https://doi.org/10.1088/1742-6596/425/18/182003>.

492 [24] R.C. Atwood, A.J. Bodey, S.W.T. Price, M. Basham, M. Drakopoulos, A high-throughput system  
for high-quality tomographic reconstruction of large datasets at Diamond Light Source, *Philos.  
Trans. R. Soc. Math. Phys. Eng. Sci.* 373 (2015) 20140398.  
495 <https://doi.org/10.1098/rsta.2014.0398>.

[25] N. Wadeson, M. Basham, Savu: A Python-based, MPI Framework for Simultaneous Processing  
of Multiple, N-dimensional, Large Tomography Datasets, *ArXiv161008015 Cs.* (2016).  
498 <http://arxiv.org/abs/1610.08015> (accessed December 29, 2021).

- [26] N.T. Vo, R.C. Atwood, M. Drakopoulos, Radial lens distortion correction with sub-pixel accuracy for X-ray micro-tomography, *Opt. Express*. 23 (2015) 32859–32868.  
<https://doi.org/10.1364/OE.23.032859>.
- [27] M.C. Strotton, A.J. Bodey, K. Wanelik, M.C. Darrow, E. Medina, C. Hobbs, C. Rau, E.J. Bradbury, Optimising complementary soft tissue synchrotron X-ray microtomography for reversibly-stained central nervous system samples, *Sci. Rep.* 8 (2018) 12017.  
<https://doi.org/10.1038/s41598-018-30520-8>.
- [28] N.T. Vo, R.C. Atwood, M. Drakopoulos, Superior techniques for eliminating ring artifacts in X-ray micro-tomography, *Opt. Express*. 26 (2018) 28396–28412.  
<https://doi.org/10.1364/OE.26.028396>.
- [29] N.T. Vo, M. Drakopoulos, R.C. Atwood, C. Reinhard, Reliable method for calculating the center of rotation in parallel-beam tomography, *Opt. Express*. 22 (2014) 19078–19086.  
<https://doi.org/10.1364/OE.22.019078>.
- [30] C.T. Rueden, J. Schindelin, M.C. Hiner, B.E. DeZonia, A.E. Walter, E.T. Arena, K.W. Eliceiri, ImageJ2: ImageJ for the next generation of scientific image data, *BMC Bioinformatics*. 18 (2017) 529. <https://doi.org/10.1186/s12859-017-1934-z>.
- [31] How to Cite Dragonfly | ORS, (n.d.). <http://www.theobjects.com/dragonfly/showcase-how-to-cite-dragonfly.html> (accessed March 19, 2020).
- [32] D. Hörl, F. Rojas Rusak, F. Preusser, P. Tillberg, N. Randel, R.K. Chhetri, A. Cardona, P.J. Keller, H. Harz, H. Leonhardt, M. Treier, S. Preibisch, BigStitcher: reconstructing high-resolution image datasets of cleared and expanded samples, *Nat. Methods*. 16 (2019) 870–874.  
<https://doi.org/10.1038/s41592-019-0501-0>.
- [33] M. Pierantoni, I. Silva Barreto, M. Hammerman, L. Verhoeven, E. Törnquist, V. Novak, R. Mokso, P. Eliasson, H. Isaksson, A quality optimization approach to image Achilles tendon microstructure by phase-contrast enhanced synchrotron micro-tomography, *Sci. Rep.* 11 (2021) 1–14. <https://doi.org/10.1038/s41598-021-96589-w>.
- [34] A. Svärd, M. Hammerman, P. Eliasson, Elastin levels are higher in healing tendons than in intact tendons and influence tissue compliance, *FASEB J.* 34 (2020) 13409–13418.  
<https://doi.org/10.1096/fj.202001255R>.
- [35] M. Pierantoni, M. Hammerman, L. Andersson, I.S. Barreto, V. Novak, H. Isaksson, P. Eliasson, Heterotopic ossification in intact rat Achilles tendons is characterized by unique mineralized collagen fiber structures, *BioRxiv*. (2022) 2022.06.28.497706.  
<https://doi.org/10.1101/2022.06.28.497706>.
- [36] K.R. Wong, R. Mychasiuk, T.J. O'Brien, S.R. Shultz, S.J. McDonald, R.D. Brady, Neurological heterotopic ossification: novel mechanisms, prognostic biomarkers and prophylactic therapies, *Bone Res.* 8 (2020) 1–14. <https://doi.org/10.1038/s41413-020-00119-9>.
- [37] F.S. Kaplan, E.M. Shore, Progressive Osseous Heteroplasia, *J. Bone Miner. Res.* 15 (2000) 2084–2094. <https://doi.org/10.1359/jbmr.2000.15.11.2084>.
- [38] J.T. Rodgers, K.Y. King, J.O. Brett, M.J. Cromie, G.W. Charville, K.K. Maguire, C. Brunson, N. Mastey, L. Liu, C.-R. Tsai, M.A. Goodell, T.A. Rando, mTORC1 controls the adaptive transition of quiescent stem cells from G0 to GAlert, *Nature*. 510 (2014) 393–396.  
<https://doi.org/10.1038/nature13255>.
- [39] G. Chen, H. Jiang, X. Tian, J. Tang, X. Bai, Z. Zhang, L. Wang, Mechanical loading modulates heterotopic ossification in calcific tendinopathy through the mTORC1 signaling pathway, *Mol. Med. Rep.* 16 (2017) 5901–5907. <https://doi.org/10.3892/mmr.2017.7380>.
- [40] J. Fu, J. Zhang, T. Jiang, X. Ao, P. Li, Z. Lian, C. Li, X. Zhang, J. Liu, M. Huang, Z. Zhang, L. Wang, mTORC1 coordinates NF-κB signaling pathway to promote chondrogenic differentiation of tendon cells in heterotopic ossification, *Bone*. 163 (2022) 116507.  
<https://doi.org/10.1016/j.bone.2022.116507>.
- [41] H. Feng, W. Xing, Y. Han, J. Sun, M. Kong, B. Gao, Y. Yang, Z. Yin, X. Chen, Y. Zhao, Q. Bi, W. Zou, Tendon-derived cathepsin K-expressing progenitor cells activate Hedgehog signaling to drive

heterotopic ossification, *J. Clin. Invest.* 130 (2020) 6354–6365.  
<https://doi.org/10.1172/JCI132518>.

- 552 [42] K.M. Meek, A.J. Quantock, The Use of X-ray Scattering Techniques to Determine Corneal  
 Ultrastructure, *Prog. Retin. Eye Res.* 20 (2001) 95–137. [https://doi.org/10.1016/S1350-9462\(00\)00016-1](https://doi.org/10.1016/S1350-9462(00)00016-1).
- 555 [43] R.A. Lewis, K.D. Rogers, C.J. Hall, E. Towns-Andrews, S. Slawson, A. Evans, S.E. Pinder, I.O. Ellis,  
 C.R.M. Boggis, A.P. Hufton, D.R. Dance, Breast cancer diagnosis using scattered X-rays, *J.*  
*Synchrotron Radiat.* 7 (2000) 348–352. <https://doi.org/10.1107/S0909049500009973>.
- 558 [44] H. Elleaume, S. Fiedler, F. Estève, B. Bertrand, A.M. Charvet, P. Berkvens, G. Berruyer, T.  
 Brochard, G.L. Duc, C. Nemoz, M. Renier, P. Suortti, W. Thomlinson, J.F.L. Bas, First human  
 transvenous coronary angiography at the European Synchrotron Radiation Facility, *Phys. Med.*  
 561 *Biol.* 45 (2000) L39. <https://doi.org/10.1088/0031-9155/45/9/102>.
- [45] C. Hall, R. Lewis, Synchrotron radiation biomedical imaging and radiotherapy: from the UK to  
 the Antipodes, *Philos. Trans. R. Soc. Math. Phys. Eng. Sci.* 377 (2019) 20180240.  
 564 <https://doi.org/10.1098/rsta.2018.0240>.
- [46] M. Lohmann, H.J. Besch, W.-R. Dix, J. Metge, B. Reime, Demands on a detector for intravenous  
 coronary angiography—experience after 379 patients, *Nucl. Instrum. Methods Phys. Res. Sect.*  
 567 *Accel. Spectrometers Detect. Assoc. Equip.* 510 (2003) 126–137.  
[https://doi.org/10.1016/S0168-9002\(03\)01689-9](https://doi.org/10.1016/S0168-9002(03)01689-9).
- [47] A.F. Brooker, J.W. Bowerman, R.A. Robinson, L.H.J. Riley, Ectopic Ossification Following Total  
 Hip Replacement: INCIDENCE AND A METHOD OF CLASSIFICATION, *JBJS.* 55 (1973) 1629.
- 570 [48] A.G. Della Valle, P.S. Ruzo, V. Pavone, E. Tolo, D.N. Mintz, E.A. Salvati, Heterotopic ossification  
 after total hip arthroplasty: a critical analysis of the Brooker classification and proposal of a  
 573 simplified rating system, *J. Arthroplasty.* 17 (2002) 870–875.  
<https://doi.org/10.1054/arth.2002.34819>.
- [49] K.T. Hug, T.B. Alton, A.O. Gee, In Brief: Classifications in Brief: Brooker Classification of  
 576 Heterotopic Ossification After Total Hip Arthroplasty, *Clin. Orthop.* 473 (2015) 2154–2157.  
<https://doi.org/10.1007/s11999-014-4076-x>.
- [50] S. Korntner, N. Kunkel, C. Lehner, R. Gehwolf, A. Wagner, P. Augat, D. Stephan, V. Heu, H.-C.  
 579 Bauer, A. Traweger, H. Tempfer, A high-glucose diet affects Achilles tendon healing in rats, *Sci.*  
*Rep.* 7 (2017) 780. <https://doi.org/10.1038/s41598-017-00700-z>.
- [51] C.F. Dilling, A.M. Wada, Z.W. Lazard, E.A. Salisbury, F.H. Gannon, T.J. Vadakkan, L. Gao, K.  
 582 Hirschi, M.E. Dickinson, A.R. Davis, E.A. Olmsted-Davis, Vessel formation is induced prior to the  
 appearance of cartilage in BMP-2-mediated heterotopic ossification, *J. Bone Miner. Res.* 25  
 (2010) 1147–1156. <https://doi.org/10.1359/jbmr.091031>.
- 585 [52] C. Hwang, S. Marini, A.K. Huber, D.M. Stepien, M. Sorkin, S. Loder, C.A. Pagani, J. Li, N.D. Visser,  
 K. Vasquez, M.A. Garada, S. Li, J. Xu, C.-Y. Hsu, P.B. Yu, A.W. James, Y. Mishina, S. Agarwal, J. Li,  
 B. Levi, Mesenchymal VEGFA induces aberrant differentiation in heterotopic ossification, *Bone*  
 588 *Res.* 7 (2019) 1–17. <https://doi.org/10.1038/s41413-019-0075-6>.
- [53] A.K. Huber, N. Patel, C.A. Pagani, S. Marini, K.R. Padmanabhan, D.L. Matera, M. Said, C. Hwang,  
 G.C.-Y. Hsu, A.A. Poli, A.L. Strong, N.D. Visser, J.A. Greenstein, R. Nelson, S. Li, M.T. Longaker, Y.  
 591 Tang, S.J. Weiss, B.M. Baker, A.W. James, B. Levi, Immobilization after injury alters extracellular  
 matrix and stem cell fate, *J. Clin. Invest.* 130 (2020) 5444–5460.  
<https://doi.org/10.1172/JCI136142>.
- 594 [54] C.-F. Hsieh, P. Alberton, E. Loffredo-Verde, E. Volkmer, M. Pietschmann, P. Müller, M. Schieker,  
 D. Docheva, Scaffold-free Scleraxis-programmed tendon progenitors aid in significantly  
 enhanced repair of full-size Achilles tendon rupture, *Nanomed.* 11 (2016) 1153–1167.  
 597 <https://doi.org/10.2217/nnm.16.34>.
- [55] S. McTighe, I. Chernev, Intramuscular Lipoma: A Review of the Literature, *Orthop. Rev.* 6  
 (2014). <https://doi.org/10.4081/or.2014.5618>.

600 [56] A. Ateschrang, C. Gratzner, K. Weise, Incidence and effect of calcifications after open-  
augmented Achilles tendon repair, *Arch. Orthop. Trauma Surg.* 128 (2008) 1087–1092.  
603 <https://doi.org/10.1007/s00402-007-0441-5>.